Title

Holistic Rice Straw Nanocellulose and Hemicelluloses/Lignin Composite Films

Journal

ACS Sustainable Chemistry & Engineering, 4(3)

ISSN

2168-0485

Authors

Hu, Sixiao

Gu, Jin

Jiang, Feng

et al.

Publication Date

2016-03-07

DOI

10.1021/acssuschemeng.5b00600

Peer reviewed

ACS Sustainable Chemistry & Engineering

Research Article

pubs.acs.org/journal/ascecg

Holistic Rice Straw Nanocellulose and Hemicelluloses/Lignin Composite Films

Sixiao Hu, Jin Gu,[†] Feng Jiang, and You-Lo Hsieh*

Fiber and Polymer Science, University of California−Davis, One Shields Avenue, Davis, California 95616, United States

Supporting Information

ABSTRACT: Rice straw was dewaxed and optimally separated into cellulose-rich solid and hemicelluloses/lignin (HL)-rich aqueous suspension with two 5 min alkali immersions (4% NaOH, 70 °C). Alkaline cellulose nanofibrils (ACNFs) were derived, at 36.5% yield from the original rice straw, by TEMPO-mediated oxidation and mechanical defibrillation of cellulose-rich portion whereas HL was isolated at 18.1% yield from the aqueous suspension. Aqueous HL solutions containing up to 30% ACNF as well as three other nanocelluloses, i.e., cellulose nanocrystals (CNC), TEMPO oxidized and aqueous counter collision generated CNFs (OCNF and ACCNF) were cast into films to exhibit significantly improved flexibility, transparencies, mechanical and moisture barrier properties. The structure−properties relations of these holistic composite films were analyzed systematically, in particular regarding to the types and loadings of the different nanocelluloses.

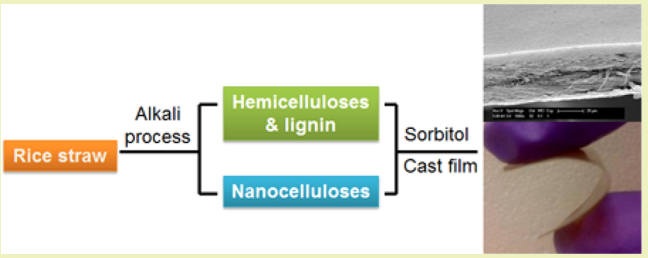

KEYWORDS: *Cellulose nanofibrils, Cellulose nanocrystals, Lignocellulose, Nanocomposites, Agricultural waste*

INTRODUCTION

Lignocellulosic biomass, especially those from agricultural and forest wastes, are abundant renewable sources for producing biobased materials to potentially replace fossil fuel based counterparts. Rice straw, at 1 to 1.5 kg per kg of rice grain harvested,[1] is among the most abundant agricultural byproducts in the world, amounting over 700 million tons in 2013.[2] Utilization of rice straw has been approached by direct conversion as well as isolation of rice straw components followed by conversion. Direct combustion of rice straw as low efficient fuel is among the easiest to implement, whereas enzymatic hydrolysis to biofuel[3,4] and pyrolysis to activated carbons[5−8] typically require multiple steps. Among the major rice straw compositions of cellulose (32−47%), hemicelluloses (19−27%), lignin (11−24%) as well as a significant amount of silica (7−20%),[9−13] cellulose has been the most studied to prepare long fibers,[14] microcrystalline cellulose,[15−17] microfibrils,[18] nanocrystals[19,20] and nanofibrils.[21−23] Rice straw hemicelluloses are mainly *O*-methyl-α-D-glucurono-L-arabino-D-xylans and glucans whereas rice straw lignin structures have been shown to contain mostly noncondensed guaiacyl and syringyl units with a smaller amount of *p*-hydroxyphenyl units.[13,24]

Hemicelluloses and lignin are intrinsically bound to each other in plant cell walls, making their separation or isolation challenging. Therefore, utilizing hemicelluloses and lignin together without separation is more desirable. In fact, hemicelluloses and lignin mixtures have demonstrated film-forming ability, which neither component alone is capable of,[25] and such films have been applied in tissue engineering,[26] drug delivery[27,28] and food packaging.[29,30] In natural plant cell walls, crystalline cellulose microfibrils are embedded in the network of amorphous hemicelluloses, whereas lignin further hardens the wall and provides structural rigidity and physical barrier. Similarly, reinforced concrete structures are engineered such that the steel core, cement and buffering material are to be analogous to the respective cellulose, lignin and hemicelluloses in plant cells.[31] Inspired by this composite structure, crystalline nanocellulose could be added in hemicelluloses/lignin matrix to improve the mechanical properties. Few works have been reported to use cellulose nanocrystals (CNCs) or nanofibrils (CNFs) as reinforcements to improve the mechanical properties, oxygen permeability and moisture barrier properties of pure xylan films.[32−38] As CNCs and CNFs differ in morphology, crystallinity as well as surface charge and functional groups, the properties of the films would be influenced and fine-tuned by careful choice of the types and loadings of nanocelluloses.[39]

The goal of this study is to develop novel composite films utilizing all lignocellulosics in rice straw. An efficient alkali process has been devised to optimize the isolation of alkaline cellulose and hemicelluloses/lignin (HL) from rice straw. The alkali processed cellulose was 2,2,6,6-tetramethylpyperidine-1-oxyl (TEMPO)-oxidized to alkaline nanocellulose fibrils (ACNFs). As nanocellulose characteristics have shown to affect composite properties,[39] the structure−property relationships in

Received: June 29, 2015
Revised: December 23, 2015
Published: January 15, 2016

DOI: 10.1021/acssuschemeng.5b00600
ACS Sustainable Chem. Eng. 2016, 4, 728−737

these films were closely examined with varying loading and types of nanocellulose, all derived from rice straw. Loadings of 10 to 30% ACNFs were studied and compared with three other rice straw nanocelluloses, i.e., sulfuric acid hydrolyzed CNCs,[22] TEMPO oxidized OCNFs[21] and aqueous counter collision generated ACCNFs[40] from pure cellulose derived from sodium chlorite-alkaline extraction process.[19] The endeavor to isolate rice straw lignocellulosic components and reconstruct into nanocellulose filled and holistic biocomposite films is to demonstrate the potential of re-engineering agricultural residues into advanced materials.

MATERIALS AND METHODS

Materials. Rice straw (Calrose variety) was harvested in the Sacramento valley in 2009. All chemicals, i.e., toluene (certified ACS, Fisher Scientific), ethanol (anhydrous, histological grade, Fisher Scientific), hydrochloric acid (HCl, 1 N, Fisher Scientific), sodium hydroxide (NaOH, 1 N, Fisher Scientific), sodium hypochlorite (NaClO, 10.6%, reagent grade, Sigma-Aldrich), 2,2,6,6-tetramethylpyperidine-1-oxyl (TEMPO, 99.9%, Sigma-Aldrich), sodium bromide (NaBr, BioXtra, 99.6%, Sigma−Aldrich) and sorbitol (laboratory grade, Fisher Scientific) were used as received. Pure rice straw cellulose was obtained by three-step dewax-sodium chlorite oxidation-alkaline leaching process[19] and used to extract other types of nanocellulose, i.e., cellulose nanofibrils from TEMPO oxidation (5 mmol/g NaClO/cellulose) (OCNF)[21] and aqueous counter collision (ACCNF) treatment (180 MPa, 30 passes, centrifuged at 14000 rpm for 15 min),[40] cellulose nanocrystals (CNC) from sulfuric acid hydrolysis (64% H_2SO_4, 45 °C, 45 min).[22] Water was purified using a Milli-Q Plus water purification system (Millipore Corporate, Billerica, MA). All percentages are wt % unless specified otherwise.

Preparation of Rice Straw Hemicelluloses/Lignin and Cellulose Nanofibrils. The major rice straw components, i.e., cellulose and hemicelluloses/lignin (HL), were isolated in sequence and all yields were reported as percentage of the original rice straw mass, at 0.1 mg accuracy (BP 300S, Satorius). Rice straw (30 g) was washed, dried and milled (Thomas-Wiley Laboratory Mill model 4, Thomas Scientific, USA) to pass through mesh 60. The milled rice straw powder was Soxhlet extracted with toluene/ethanol (2:1, v/v, 450 mL) at 150 °C for 24 h to remove wax, pigments and oils. The dewaxed rice straw powder was treated with 4% NaOH at a 15 mL/g liquid to solid ratio at 70 °C for 5 min, centrifuged (5000 rpm, 15 min), washed with water five times and filtered. This alkaline process was repeated with fresh 4% NaOH a second time and the powder was washed with water until the rinse pH reached neutral and filtered to give the cellulose-rich solid. The two filtrates from repeated alkali treatments were combined and neutralized with 1 N HCl and centrifuged (5000 rpm, 15 min) to precipitate silica. The supernatant was dialyzed in water for 3 days to remove all the salts then freeze-dried to obtain HL.

The cellulose-rich solid was TEMPO oxidized and mechanically defibrillated following a previously reported procedure to generate alkaline isolated cellulose nanofibril (ACNF).[21] Oxidation was initiated by adding 7.5 mmol NaClO dropwise to 100 mL of aqueous mixture containing 1 g of freeze-dried cellulose-rich solid, 0.016 g of TEMPO and 0.1 g of NaBr at pH 9.8−10.2 (OAKTON pH/Con 510 series meter) adjusted by 0.5 M NaOH at ambient condition (21 °C, 1 atm) until no further pH decrease. The suspension was neutralized with 0.5 M HCl, centrifuged (5000 rpm, 15 min), dialyzed against water to remove salts and other small molecules, mechanical defibrillated using a household blender (Vitamix 5200, 37000 rpm, 30 min) and then centrifuged again (5000 rpm, 15 min) to obtain the ACNF containing supernatant.

Preparation of HL Composite Films. The composite films were prepared by mixing HL, sorbitol and nanocelluloses. The sorbitol loading was always fixed at 30%, whereas the ACNFs loading were 0, 10, 20 and 30% with the remaining to be HL. Those composite films were designated as 7/3 HL/S, ACNF10, ACNF20, ACNF30, respectively. The mixtures were heated at 80 °C and concentrated to 10 mg/mL. The solution of 10 mL was cast into films on polystyrene dishes and dried under the ambient condition (21 °C, 1 atm). Hemicelluloses and lignin were also cast into HL films with a constant 20% OCNF, CNC and ACCNF and designated as OCNF20, CNC20 and ACCNF20, respectively. All films had uniform thickness of ca. 50 μm and were stored at 23 °C, 60% humidity before testing.

Analytical Methods. *Surface Morphology and Charges of ACNF.* ACNF (10 μL, 0.0005%) was deposited onto freshly cleaved mica, dried at ambient temperature of 21 °C and imaged with an atomic force microscopy (AFM, Asylum-Research MFP-3D) in tapping mode using a OMCL-AC160TS standard silicon probe. The surface charge of ACNF was characterized by conductometric titration. 50 mL of 0.1% ACNF suspension was protonated by adding excessive 1 N HCl, then titrated with 0.02 M NaOH solution. The conductivity of the suspension (measured by OAKTON pH/Con 510 series meter) and the volume of NaOH consumed were recorded. The total carboxylic/carboxylate content (σ, in mmol per gram of cellulose) was determined by eq 1, where c is the NaOH concentration (0.02 M), m is the mass of ACNF (50 mg), and v_1 and v_2 are NaOH volumes (in mL) used from neutralizing the excessive HCl and total acid groups, respectively.

$$\sigma = \frac{cv}{m} = \frac{c(v_2 - v_1)}{m} \quad (1)$$

Chemical and Thermal analysis of ACNF and HL. The chemical structures of ACNF and HL were characterized by Fourier transform infrared spectroscopy (FTIR) (Nicolet 6700, Thermo Scientific). Each sample was pressed with anhydrous KBr powders into pellets and stored at 60 °C for 24 h before measurements. The thermal properties of HL were analyzed by differential scanning calorimetry (DSC) (DSC-60, Shimadzu) and thermogravimetric analysis (TGA) (TGA-50, Shimadzu). DSC samples were tightly packed in aluminum cells with press-sealed lids, whereas TGA samples were placed in platinum pan. HL samples were heated at 10 °C/min to 500 and 600 °C for DSC and TGA, respectively, under 50 mL/min nitrogen flow.

Morphological and Structural Analysis of Composite Films. The optical transmittance of the composite films was measured by ultraviolet−visible spectroscopy (UV−vis) (Evolution 600, Thermo Scientific). The composite films were cut into 2 cm × 5 cm pieces and placed in the UV sample holder for measurements. The hand broken cross sections of the films were observed using a scanning electron microscope (SEM) (FEI-XL 30, FEI) and the elemental compositions were evaluated by energy-dispersive X-ray spectroscopy (EDX, X-Max^N Silicon Drift Detector, Oxford Instruments, Abingdon, Oxfordshire, England) adjunct to a SEM. The surface morphology and roughness of the films were characterized by SEM and AFM, by adhering the films flat onto to aluminum support and glass slide, respectively, using carbon tapes. The root mean square (RMS) roughness was calculated based on scanning over a 15 μm × 15 μm area on the AFM images. The crystalline structures of freeze-dried nanocellulose and HL powder and cast HL films were obtained with a Scintag XDS 2000 powder X-ray diffractometer using a Ni filtered Cu Kα radiation generated at 45 kV and 40 mA. Diffractograms were collected at a rate of 2° /min from 5 to 40° 2θ. The crystallinity of nanocellulose was calculated using an empirical equation:[41]

$$\mathrm{CrI} = \frac{I_{200} - I_{\mathrm{am}}}{I_{200}} \times 100 \quad (2)$$

where I_{200} and I_{am} are the intensity of the 200 peak (2θ = 22.7°) and amorphous peak (2θ = 18.7°), respectively. The crystallite size (200 plane) of the nanocelluloses were calculated based on the Scherrer equation:[42]

$$B_{200} = \frac{K\lambda}{\cos\theta\Delta 2\theta} \quad (3)$$

where B_{200} is the crystal width of (200) plane; K is a constant (K = 0.9); λ is the wavelength of incident X-rays (λ = 0.154 06 nm); θ is the corresponding Bragg angle (2θ = 22.7°); $\Delta 2\theta$ (in radius) is the fwhm

DOI: 10.1021/acssuschemeng.5b00600
ACS Sustainable Chem. Eng. 2016, 4, 728−737

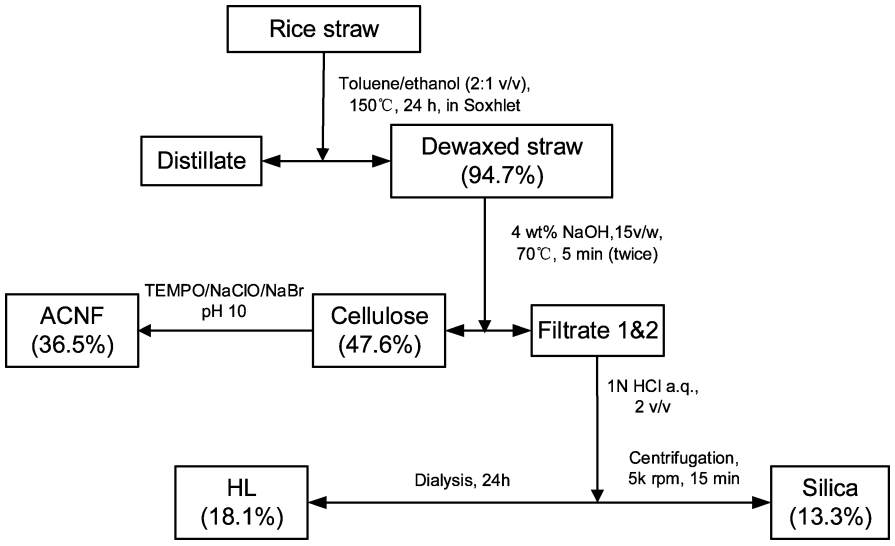

Figure 1. Flowchart showing the preparation process and yield of ACNFs and HL.

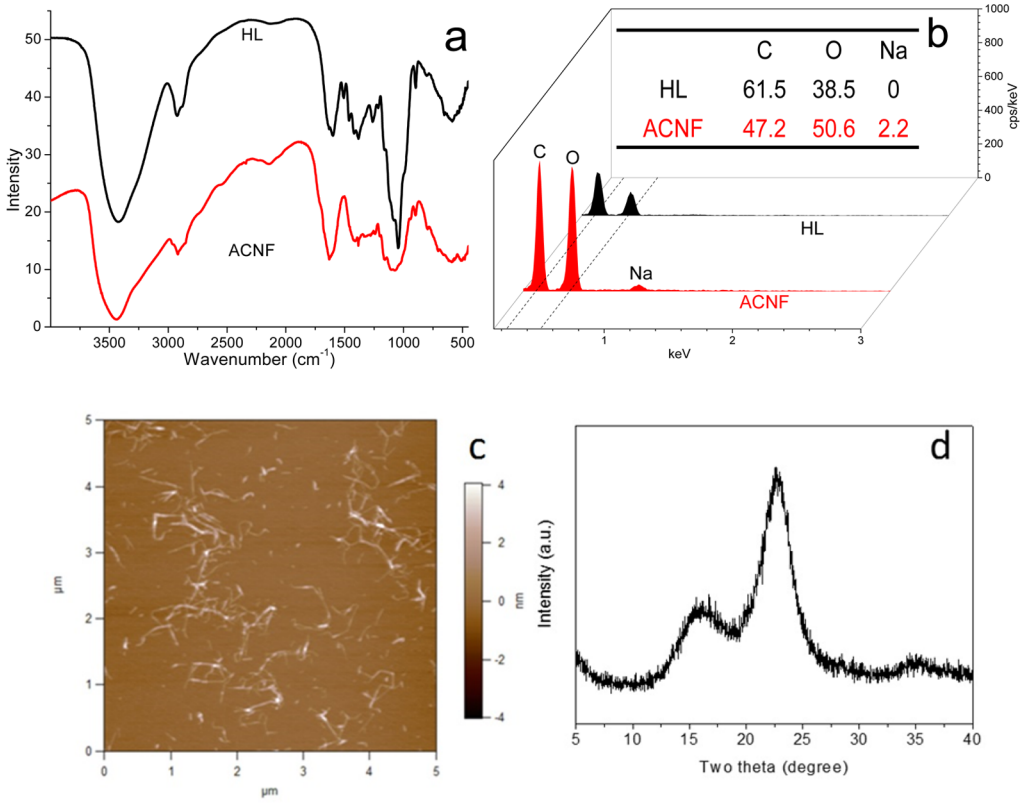

Figure 2. Characterization of ACNF and HL: (a) FTIR spectra; (b) EDX spectra; (c) AFM image and (d) XRD diffractogram of ACNFs. The inset table in panel b shows carbon, oxygen and sodium mass contents in percentage.

of the 200 peak and it is determined by peak deconvolution using Peakfit (www.sigmaplot.com).

Mechanical Analysis of Composite Films. The tensile properties of HL composite films were measured on an Instron tensile tester (model 5566) fitted with a pair of pneumatic grips. The films with typical thickness of 50 μm were cut into 5 mm wide and 30 mm long specimens and each film was tested in at least five replicates at a 10 mm gauge length and a constant 0.5 mm/min strain rate until break at 23 °C and 60% humidity. Ultimate tensile stress (σ) was the maximum breaking force normalized by the cross-sectional area of each sample, i.e., actual width and thickness, measured using a caliper (0.01 mm resolution, Neiko 01407A, Neiko Tools USA) and a micrometer (1 μm resolution, Mitutoyo No. 293-340, Japan), respectively. Strain (ε) at break was calculated as $\Delta L/L_0$ where L_0 is the initial gauge length (10 mm) and ΔL is the absolute difference between original and present length. Young's modulus defined by the initial slope of $\sigma-\varepsilon$ curve as well as the ultimate tensile stress and strain were averaged and the mean and standard deviation values were reported.

Water Permeability and Sorption of Composite Films. The moisture vapor transmission rate (MVTR) was measured according to ASTM E96-95. Briefly, 12 mg of water was added to a 1.833 cm diameter cylindrical bottle to be covered with 50 μm thick film of the same dimension and sealed with epoxy adhesive. The bottle was weighed under a constant 23 °C and 60% humidity environment at 10

DOI: 10.1021/acssuschemeng.5b00600
ACS Sustainable Chem. Eng. 2016, 4, 728−737

Table 1. Characteristics of All Nanocellulose used for HL Composite Film Preparation

samples	thickness (nm)	width (nm)	length (nm)	CrI (%)	crystallite size (nm)	sulfate[a], carboxylic/carboxylates[b] content (mmol/g)
CNC[52]	4.7 ± 1.3	6.4 ± 1.2	143 ± 31	90.7	4.2	0.24[a]
ACNF	1.4 ± 0.8	ND	100−1000	67.8	2.7	1.25[b]
OCNF[21]	1.5 ± 0.5	2.1 ± 0.4	100−1000	63.2	2.6	1.29[b]
ACCNF[40]	3.7 ± 1.9*	5.5 ± 1.4*	>1000	77.9	ND	N/A

*The cellulose nanofibrils with lateral dimensions of over 10 nm (c.a. 10 %) were excluded from the average thickness and width calculation.

min interval for 3 h. The linear mass loss over time was fitted using OriginPro 8.1 SR3 software to determine the slope r for calculating MVTR by eq 4:

$$\mathrm{MVTR}\left(\frac{\mathrm{g}}{\mathrm{h}}\cdot\mathrm{m}^2\right) = \frac{|r|}{\pi \times \left(\frac{0.01833}{2}\right)^2} \tag{4}$$

The film was cut from the bottle using a razor blade right after the MVTR measurements and weighed immediately (m_1) and then again (m_0) after conditioning under constant 23 °C and 60% humidity for 2 days. The moisture content was calculated by eq 5:

$$\text{moisture content or water uptake} = \frac{m_1 - m_0}{m_0} \times 100\% \tag{5}$$

The water sorption curves of HL composite films were measured with 0.01 mg resolution using Kruss tensiometer K100 (Kruss, Hamburg Germany). Each 3 mm wide and 12 mm long film was hung vertically with the lower edge brought in contact with 50 mL water in a glass vessel for water sorption measurement for 30 min, then measured again after removing from water.

For water uptake and swelling, each HL composite film (1−2 mg) was weighed (m_0) and thickness measured (h_0) then completely immersed in water for 30 min. The wet specimen was removed from water and dapped with Kimwipes to remove surface excess water and weighed (m_1) and thickness measured (h_1) again. The water uptake and swelling ratio were determined from eqs 5 and 6, respectively.

$$\text{swelling ratio} = \frac{h_1 - h_0}{h_0} \times 100\% \tag{6}$$

RESULTS AND DISCUSSION

Preparation and Characterization of ACNF and HL. Extraction with toluene/ethanol (2:1 (v/v), 150 °C, 24 h) removed 5.3% organic soluble components. The brief double alkali treatments (4% NaOH, 70 °C, 5 min) dissolved silica and most of hemicelluloses and lignin (HL), yielding 47.6% cellulose-rich solid (Figure 1). The combined dark brown alkali filtrate was neutralized to precipitate 13.3% silica, similar to 15.3% previously reported,[20] and 18.1% HL upon dialysis and freeze-drying, all together accounting for 84.3% of rice straw. The remaining 15.7% include moisture, minerals and loss from washing and dialysis. The light yellow cellulose, indicative of residual lignin, was then subjected to TEMPO oxidation and mechanical defibrillation to produce alkali derived cellulose nanofibrils (ACNFs) at 77% of the cellulose-rich solid or 36.5% of rice straw. The mass reduction from TEMPO oxidation-defibrillation process was attributed to the loss of oxidized lignin, hemicelluloses and amorphous cellulose. The white color of ACNFs indicated the eventual dissolution and removal of lignin.

The FTIR of HL and ACNF exhibited characteristic peaks of hemicelluloses/lignin and cellulose, respectively (Figure 2a). Both spectrum showed common lignocellulose peaks: broad hydroxyl stretching at 3425 cm^{-1} and bending at 1630 cm^{-1}, predominant C—O peak at 1045 cm^{-1}, as well as two minor asymmetric $-CH_2$ and symmetric $-CH_3$ stretching peaks at 2930 and 2870 cm^{-1}, respectively. The presence of lignin in HL was evident by the skeletal stretching of aromatic ring at 1600 and 1505 cm^{-1}, the benzene C═C stretching at 1460 cm^{-1}, as well as the aromatic ring breathing with C═O at 1260 cm^{-1}. These lignin peaks resembled those derived from softwood via commercial alkali pulping process.[43]

The EDX elemental analysis of HL showed 61.5% C and 38.5% O in mass (Figure 2b) with C content in between that of lignin (58 to 65%)[44−46] and hemicelluloses (38 to 42%).[44,47] ACNF consisted of 47.2% C, 50.6% O and 2.2% Na in mass, with a 1.24 C/O atomic ratio very close to the 1.2 C/O ratio of pure cellulose. The chemical composition analysis confirmed the complete removal of silica and manifested the efficiency of this ACNF production process from rice straw. The presence of sodium in ACNF confirmed sodium carboxylates expected from TEMPO oxidation.

The TGA (Figure S1) showed HL was relatively hygroscopic with 9.5% moisture content. The HL mass was stable at up to 210 °C, and then rapidly decreased to 37% at 375 °C and eventually to 21% at 600 °C. The two stage mass losses corresponded to two major exotherms at 310 and 455 °C, indicative of the respective hemicelluloses and lignin decomposition. Assuming complete decomposition of hemicelluloses into volatiles and 60% alkali lignin char at 600 °C,[43] HL was estimated to contain 65% hemicelluloses and 35% lignin, similar to their proportion in raw rice straw.

The AFM height image showed ACNFs to be less than 5 nm thick and a few hundred nanometers to several micrometers long (Figure 2c). The X-ray diffraction of freeze-dried ACNF showed two peaks at 2θ 16.0 and 22.7°, typical cellulose Iβ crystalline structure (Figure 2d), and 67.8% crystalline. The total surface carboxylate/carboxylic content of ACNF was determined to be 1.25 mmol/g of cellulose or 0.202 per anhydroglucose (AG) (Table 1).

The structure and characteristics of three rice straw nanocelluloses were also compared (Table 1). CNCs were most crystalline (CrI = 90.7%), but widest (4−6 nm) and shortest with the lowest aspect ratios (20−30) whereas both OCNFs and ACNFs had smallest lateral dimensions of 1.4−2.1 nm but highest lengths and aspect ratios as well as lowest crystallinity of 63.2−67.8%. ACCNFs were most heterogeneous with the smaller ones averaged 3.7 nm thick and 5.5 nm wide, similar to CNCs in lateral dimensions, but longer than OCNFs and ACNFs. Approximately 10% of ACCNFs were much wider in the 10−20 nm range. Except for the uncharged ACCNFs from mechanical defibrillation, all other nanocelluloses were negatively charged. CNCs had 0.24 mmol sulfate per g whereas OCNFs and ACNFs contained 1.29 and 1.25 mmol carboxylate/carboxylic per g, respectively.

Film Topology and Internal Structures. Aqueous suspension of HL alone could be cast into intact films, but the films were brittle and easily fractured upon handling. Adding 30% sorbitol as a plasticizer, the brownish 7/3 HL/S film was flexible and uniform without any visible aggregations.

DOI: 10.1021/acssuschemeng.5b00600
ACS Sustainable Chem. Eng. 2016, 4, 728−737

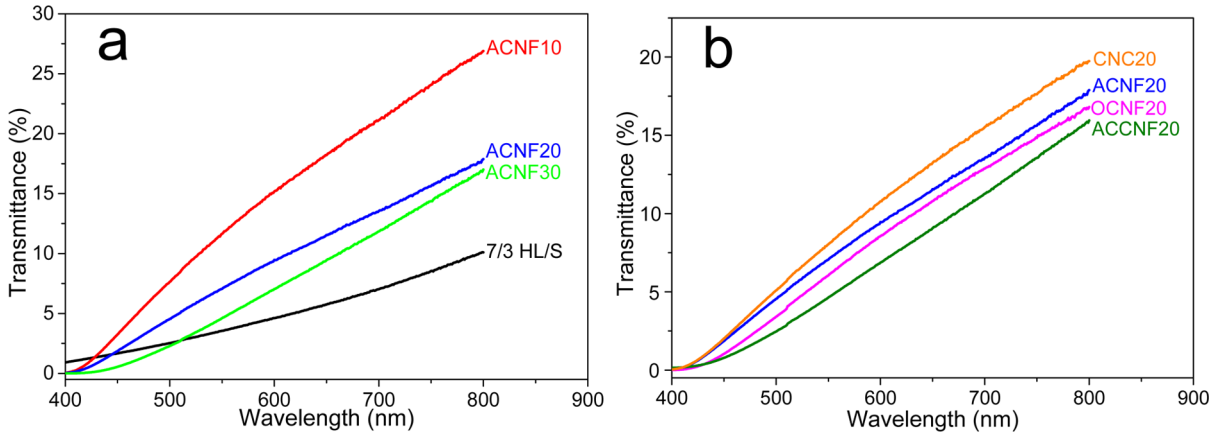

Figure 3. UV−vis transmittance of HL composite films reinforced with (a) ACNF at varied contents; (b) CNC20, ACNF20, OCNF20, and ACCNF20 nanocelluloses.

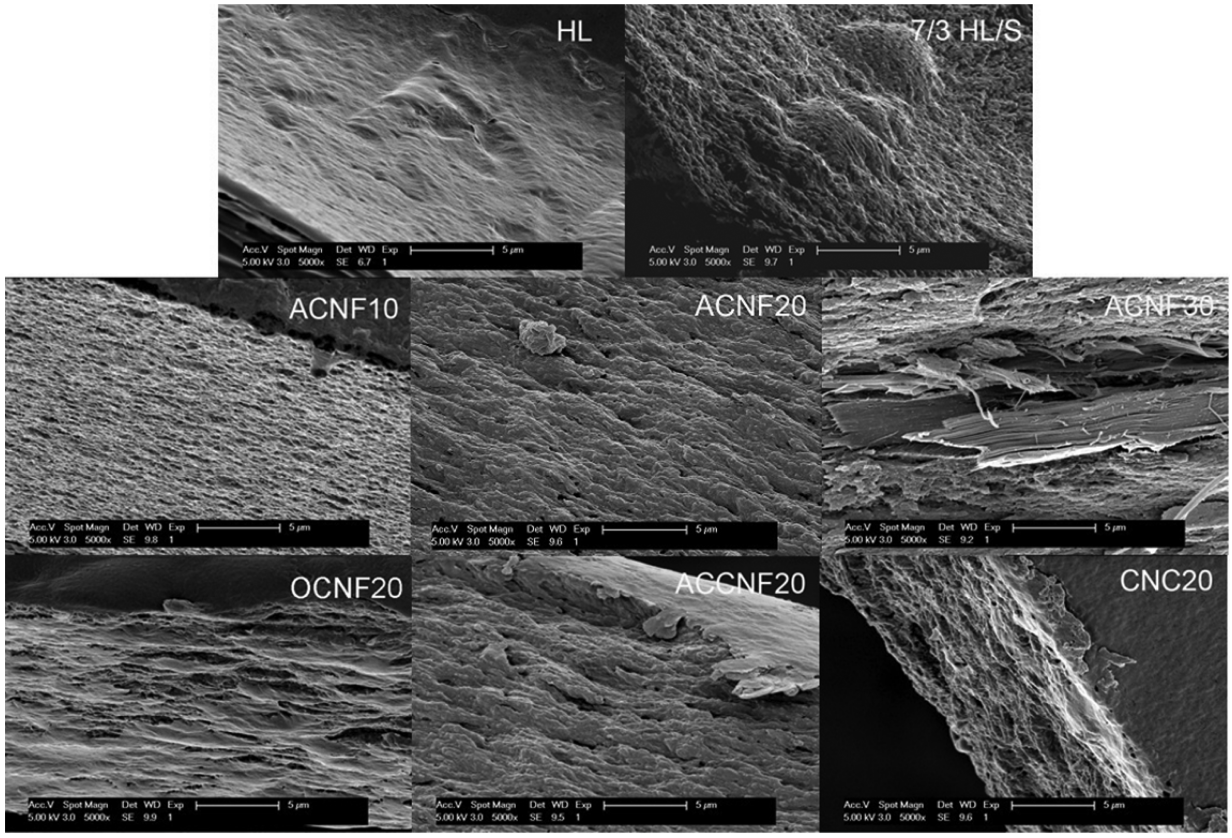

Figure 4. SEM of films cross sections (bar = 5 μm).

The 7/3 HL/S film appeared opaque with 1−10% optical transmittance at the 400−800 nm wavelength range, and the visible light transmission was dramatically increased to up to 27% for ACNF10 film (Figure 3). The improved optical transmittance of ACNF10 film is expected considering the high transparency of ACNF itself. However, the optical transmittance lowered slightly to up to 18 and 17% for ACNF20 and ACNF30 film, respectively, suggesting ACNF aggregation at higher loadings. The optical transmittance of other nanocellulose loaded films was also improved, so was their flexibility. At the same 20% nanocellulose loading, films containing CNC had the highest optical transmittance of up to 20%, due to the lack of entanglement and aggregation of the shortest CNCs, whereas those with ACNF and OCNF showed slightly lower optical transmittance, again indicating aggregation of these longer nanofibrils. The lowest optical transmittance of ACCNF20 is consistent with its largest and most heterogeneous dimensions. Nevertheless, the optical transmittance of nanocellulose loaded composite films is more than 2 or 3 times of that for 7/3 HL/S, manifesting the beneficial effect of nanocellulose in improving the transparency of the composite films.

All films had 22 to 79 nm surface RMS roughness (Figure S2). The sorbitol plasticizer slightly increased the roughness from 22.7 to 27.4 nm, possibly due to the phase separations between sorbitol and HL. Incorporation of 10% ACNF

DOI: 10.1021/acssuschemeng.5b00600
ACS Sustainable Chem. Eng. 2016, 4, 728−737

introduced further phase separations between the nanocelluloses, sorbitol and HL, and increased the film RMS to 42.5 nm. Further increasing ACF contents to 20 and 30% slightly lowered RMS to 39.6 and 36.7 nm, respectively. Although similar undulated surfaces were observed on all ACNF loaded HL/S films, showing no difference with increasing loadings (Figure S3a−e), a fibrous structure was clearly observed on surface of the film containing 30% ACNF at a 45° tilt (Figure S3f), showing surfacing of the long CNFs from the HL/S matrix. The formation of such continuous nanocelluloses web might mitigate the phase separations and led to slightly smoother surface as indicated by RMS values. The relative smooth surfaces of all ACNF filled HL/S composite films suggested excellent interfacial compatibility between HL, sorbitol and nanocelluloses, owning to the extensive hydrogen bondings among these components, all containing aboundant hydroxyl groups.

The different nanocelluloses at the same 20% loading posed different effects on surface roughness. The OCNF20 composite film had similar roughness of 44.9 nm as that of ACNF20, whereas ACCNF20 film had a significantly rougher surface with RMS of 78.7 nm and surface particulates as seen by SEM (Figure S4), consistent with the larger and more heterogeneous ACCNFs as compared to other nanocelluloses (Table 1). In contrast, the CNC20 film had the smoothest surface with lowest RMS of 26.6 nm, essentially the same as 7/3 HL/S film. The much shorter, less surface charged and more rigid CNCs appeared to be more homogeneously integrated with hemicellulose/lignin to give the smoothest surface.

The fractured cross sections of HL films appeared densely compact and relatively featureless whereas that of 7/3 HL/S film was less dense, showing grain-like internal structure (Figure 4). The internal morphologies of nanocellulose filled films, in particular those with nanofibrils, were significantly altered. The ACNF filled films exhibited a porous fibrillar structure at 10% loading and were more compact with denser fibrillar layers at higher loadings, with the 30% ACNF filled film clearly showed layered nanofibrillar structures at the fractured cross section. These observations indicated the self-assembly of nanofibrils into submicron fibers and then micron-sized layers ~~as~~with increasing ACNF loadings. Similarly, the composite films containing 20% OCNF and ACCNF also exhibited densely layered structures on their fractured surfaces. These observations on internal structures were consistent with the previous topology analysis. The thinner and longer CNFs tend to self-assemble into larger fibers and layered structures.

Crystalline Structure. HL powder was amorphous, showing a broad scattering centered at 2θ = 20°. 7/3 HL/S film exhibited a peak at 2θ = 18° and a small shoulder at 2θ = 21° (Figure 5), indicative of its partially crystalline structure, likely from the crystallinzation of xylan-rich hemicelluloses of rice straw as neither amorphous lignin nor sorbitol less than 50%[35,48] could impose crystalline structural change. Depending on the extraction methods and sources, rice straw hemicelluloses have shown to consist of 32−60% xylan, 8−43% glucan and a small amount of arabinan and galactan.[13,24] The major hemicellulose was structurally defined as 4-*O*-methyl-α-D-glucurono-L-arabino-D-xylans.[13,24] The crystalline peaks at 18 and 21° are consistent with those previously reported at 17−18 and 21−23° for xylans with low degree of substitution, which crystallize via interchain hydrogen bonds.[35,48−50] With 20% nanocelluloses, the cellulose I characteristics peaks at around 2θ = 16.0 and 22.7° were clearly observed on all films and the peak

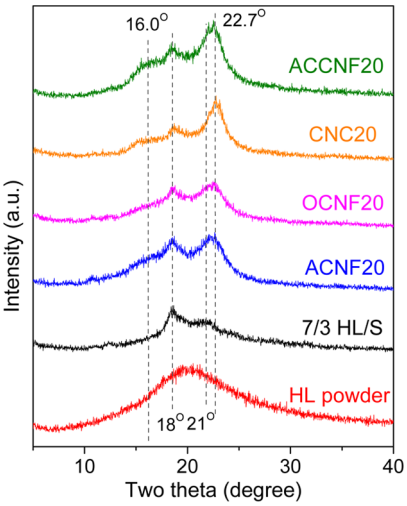

Figure 5. X-ray diffraction patterns of freeze-dried HL powder, 7/3 HL/S, ACNF20, OCNF20, CNC20 and ACCNF20 films.

at 2θ = 22.7° intensified with increasing ACNF contents (Figure S5), similar to the effect of softwood microfibrillated cellulose on the crystallinity of rye arabinoxylan films.[34]

Tensile Properties. The low Young's modulus (167 MPa) and tensile stress (6.4 MPa) of 7/3 HL/S film were markedly enhanced by ACNF (Figure 6) reinforcements. With 10% ACNF, the Young's modulus was slightly increased by 11%, and the tensile stress and strain at break were more greatly improved by 53% and 155%, respectively, whereas doubling ACNF content to 20% significantly increased the Young's modulus and tensile stress by 184% and 236%, respectively, and 85% higher in strain at break. As the ACNF content increased to 30%, the Young's modulus dramatically increased by four times to 700 MPa, whereas the tensile strength was enhanced by 266% to 23.4 MPa, but the strain at break dropped to 12.4%, similar to 7/3 HL/S film. Therefore, the modulus of HL/S film was significantly improved with increasing loadings of ACNFs from 10 to 30%, whereas the tensile strength and strain were optimized at 20%.

Although hemicelluloses alone from various plant sources could not form self-supporting films,[25,51] rice straw HL with ca. 65% hemicelluloses and 35% lignin is film-forming without a plasticizer, possibly due to plasticizing effect of lignin as reported in cotton stalk xylan film containing lignin[25] and sorbitol further enhanced film flexibility. The 7/3 HL/S film had comparable mechanical properties as bamboo xylan film containing 25% sorbitol with 11.9 MPa tensile strength and 3.4% strain at break.[35] ACNFs enhanced the mechanical performance of 7/3 HL/S film, possibly via strong interfacial hydrogen bonding. The flexible ACNF possibly increased the coherence of the films during the stretching process and thus increase the strain at break at a low loading of 10%. Increasing ACNF content to 20% showed an interconnecting nanofibrils network in the HL matrix in SEM in which stress transfer through CNF−CNF interactions may occur. These stress transfer between the ACNF reinforcement and HL matrix seems to be confirmed by the limited exposure of ACNFs at the fracture (Figure 4).[34]

Most impressively, all nanocelluloses had two to 4 times increase in the Young's modulus and tensile strength, and both ACNF20 and OCNF20 showed nearly double tensile strain of the 7/3 HL/S film (Figure 6 and Table 2). Although ACNF

DOI: 10.1021/acssuschemeng.5b00600
ACS Sustainable Chem. Eng. 2016, 4, 728−737

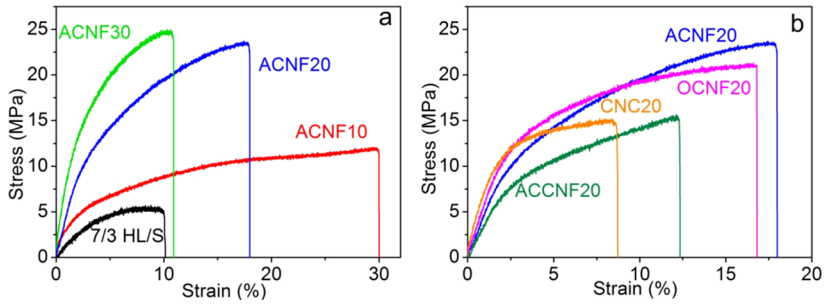

Figure 6. Typical stress–strain curves of HL composite films reinforced with (a) ACNF at varied contents; (b) varied nanocelluloses.

Table 2. Tensile Properties of Nanocellulose Reinforced HL Composite Films

samples	Young's modulus (MPa)	tensile strength (MPa)	strain at break (%)
7/3 HL/S	167 ± 46	6.4 ± 1.3	10.9 ± 2.4
ACNF10	186 ± 28	9.8 ± 0.8	27.8 ± 4.5
ACNF20	475 ± 94	21.5 ± 3.0	20.2 ± 4.6
ACNF30	700 ± 50	23.4 ± 4.7	12.4 ± 3.9
OCNF20	487 ± 137	18.3 ± 4.1	15.8 ± 3.2
ACCNF20	383 ± 91	15.7 ± 2.7	13.9 ± 1.8
CNC20	593 ± 94	13.1 ± 1.9	10.5 ± 1.8

Table 3. Moisture Properties, Water Uptake and Swelling Ratio of Nanocellulose Reinforced HL Composite Films*

film	MVTR (g/h·m^2)	moisture content (wt %)	water uptake (wt %)	swelling ratio (%)
7/3 HL/S	45.7	7.0	dissolved	dissolved
ACNF10	74.6	10.3	1417	789
ACNF20	43.8	6.6	4100	2661
ACNF30	35.4	5.9	5836	4822
OCNF20	55.2	7.5	3554	2562
ACCNF20	61.3	4.9	1014	787
CNC20	40.2	4.8	dissolved	dissolved

*All films were ca. 50 μm thick.

and OCNF had comparable dimensions and surface COOH/COO^- content, films filled with ACFs have slightly higher strength and strain at break than those of OCNF20, likely due to the residual lignin/hemicelluloses in ACNFs giving higher affinity to the HL matrix. CNC20 produced the highest Young's modulus of 593 MPa, but lowest tensile strength and strain at break whereas ACCNF20 enhanced Young's modulus the least among all nanocellulose, but still more than double those of the 7/3 HL/S film. The most crystalline CNCs (90.7%) were theoretically the strongest and most homogeneous mixed with the HL matrix to give the films the highest Young's modulus among all nanocelluloses at 20% loading, but the strength of CNC-filled films were limited by their low aspect ratio and lacking evidence of any association among CNCs. The most heterogeneous and uncharged ACCNF had less significant reinforcing effects than the thinner and surface carboxylated OCNF and ACNF, however, still produced slightly higher tensile strength and strain than CNC20 film. Although all nanocellulose improved tensile strength of their filled biocomposite films, highest modulus was achieved with the strongest and most homogeneous mixed rigid CNCs whereas highest tensile strength and elongation were found with the thinnest and longest CNFs, in particular ACNFs that contain residual lignin/hemicelluloses. These comparative tensile properties show clear association of geometries, crystallinity and surface chemistry of nanocelluloses with their reinforcing effects in the HL matrix.

Water Vapor Permeability and Water sorption. Incorporating 10% ACNF significantly increased the vapor transmission rate (MVTR) of HL/S film from 45.7 to 74.6 g/h·m^2 and moisture absorption from 7% to 10.3%, whereas 20% CNC lowered both moisture properties (Table 3). Further increasing ACNF contents to 20 and 30% decreased both the MVTR (43.8 and 35.4 g/h·m^2) and moisture absorption (6.6% and 5.9%). This was due to the increasing replacement of the more heterogeneous and hygroscopic HL/S with highly crystalline ACNFs, even with their hydrophilic surfaces. Furthermore, CNFs self-assembled into fibers and more structured layers with increasing loadings, lowering moisture transmission. Again, both TEMPO oxidized ACNF and OCNF had similar moisture properties and behavior in water due to their similar dimensions and surface oxidation.

The 7/3 HL/S film absorbed water immediately upon immersion and then dissolved in water in 84 s (Figure 7a). ACNF films continued to absorb water over time without dissolving, demonstrating improved stability in water. However, all films swelled significantly at the end of sorption with increased weight gain as ACNF content increased, indicating hygroscopic nature of these lignocellulosic films. The water sorption result was consistent with the water uptake of 1417, 4100 and 5836% and swelling ratio of 789, 2661 and 4822% for ACNF10, ACNF20 and ACNF30, respectively (Table 3). The improved water stability by incorporating ACNF could be due to formation of interconnected nanocellulose networks with entanglement of long ACNF, as evidenced from SEM images. Besides, the increased water uptake and swelling ratio at higher ACNF contents indicated that ACNF was responsible for water sorption, likely through hydrogen bonding of water with surface hydroxyls and negatively charged carboxylate groups, latter of which could ionize when exposed to water and repel each other, resulting in film swelling. Among all nanocelluloses, CNC20 film showed fastest water sorption, similar to 7/3 HL/S film but a much delayed dissolution time of 1400 s (Figure 7b). The extents of water sorption of CNF films were ACNF20 ≈ OCNF20 > ACCNF20, consistent with 4100, 3554, and 1014% water uptake and 2661, 2562 and 787% swelling ratios, respectively.

Nanocellulose crystallinity, surface areas and surface charges all could affect moisture and water absorption, and the aspect ratios could influence water stability. The low moisture absorption of CNCs could be ascribed to its higher crystallinity and relatively lower specific surface due to its larger lateral dimensions (Table 1), leading to less available surface hydroxyls to bind water, whereas its low water stability could

DOI: 10.1021/acssuschemeng.5b00600
ACS Sustainable Chem. Eng. 2016, 4, 728–737

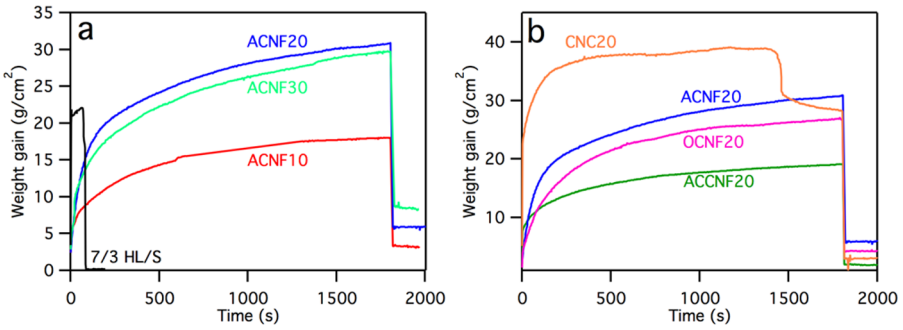

Figure 7. Water sorption curves of HL composite films reinforced with (a) ACNF at varied contents; (b) CNC20, ACNF20, OCNF20 and ACCNF20 nanocelluloses.

be due to the low aspect ratio that could not intertwine with each other to form strong network structures. The low moisture absorption, water uptake and swelling of ACCNF reinforced film may have to do with their highly branched fibrillated structure and uncharged surfaces, as well as lower surface area. Because both ACNF and OCNF were similar in dimensions and containing comparable amount of carboxylate, their moisture absorption and water uptake and swelling were similar to each other.

CONCLUSIONS

A facile two brief immersions in 4% NaOH (70 °C, 5 min) were effective in isolating rice straw into cellulose-rich solid and aqueous suspension for the preparation alkaline cellulose nanofibrils (ACNFs) and hemicellulose and lignin (HL) at 36.5 and 18.1% yields, respectively. The HL films plasticized by 30% sorbitol were reinforced with ACNFs at 0−30% loadings as well as three other types of rice straw nanocelluloses, i.e., sulfuric acid hydrolyzed CNCs, TEMPO oxidized CNFs (OCNFs) and aqueous counter collision generated CNFs (ACCNFs), all at 20% loading. Nanocellulose incorporation improved transparency as well as flexibility of HL/S composite films and rendered them insoluble in water. Although water uptake and swelling increased with ACNF contents, water vapor transmission (MVTR) and moisture content increased with 10% ACNF loading, then decreased at higher loadings. The surface oxidized ACNF and OCNFs had higher affinities to moisture and water than ACCNFs. CNC20 exhibited the lowest MVTR and moisture content compared to other nanocelluloses films. ACNF enhanced the Young's modulus and tensile strength up to 319 and 266% respectively, as well as improved the strain at break. At 20% nanocellulose loading, CNC20 film exhibited the highest Young's modulus (255% increase) whereas the ACNF20 exhibited the highest improvement in tensile strength (by 236%) and strain at break (by 85%). This work, for the first time, demonstrated that nanocelluloses in parallel to hemicelluloses/lignin were efficiently isolated and reconstructed into holistic biocomposite films from a single biomass, i.e., rice straw. The structure−properties relations were clearly elucidated to show that tensile strength and elongation to be most enhanced by ACNFs where tensile modulus as well as moisture transmission and content most improved by CNC, showing great feasibility of re-engineering agricultural residues into value-added performance materials.

ASSOCIATED CONTENT

Supporting Information

The Supporting Information is available free of charge on the ACS Publications website at DOI: 10.1021/acssuschemeng.5b00600.

Thermal analysis of HL; AFM, SEM and XRD of the composite films (PDF).

AUTHOR INFORMATION

Corresponding Author

*Y.-L. Hsieh. Tel: +1 530 752 0843. E-mail: ylhsieh@ucdavis.edu.

Present Address

†College of Materials and Energy, South China Agricultural University, Guangzhou, Guangdong 510642, China

Notes

The authors declare no competing financial interest.

ACKNOWLEDGMENTS

Funding for this research from California Rice Research Board (RU-9) and USDA NIFA (2011-67021-20034) is greatly appreciated.

REFERENCES

(1) Moo-Young, M. *Comprehensive Biotechnology: The Principles, Applications, and Regulations of Biotechnology in Industry, Agriculture, and Medicine*; Moo-Young, M., Ed.; Pergamon: Oxford, U. K., 1985.
(2) (FAOSTAT), F. a. A. O. o. t. U. N., 2013.
(3) Bak, J. S.; Ko, J. K.; Han, Y. H.; Lee, B. C.; Choi, I.-G.; Kim, K. H. Improved Enzymatic Hydrolysis Yield of Rice Straw Using Electron Beam Irradiation Pretreatment. *Bioresour. Technol.* **2009**, *100*, 1285−1290.
(4) Binod, P.; Sindhu, R.; Singhania, R. R.; Vikram, S.; Devi, L.; Nagalakshmi, S.; Kurien, N.; Sukumaran, R. K.; Pandey, A. Bioethanol Production from Rice Straw: An Overview. *Bioresour. Technol.* **2010**, *101*, 4767−4774.
(5) An, D.; Guo, Y.; Zou, B.; Zhu, Y.; Wang, Z. A Study on the Consecutive Preparation of Silica Powders and Active Carbon from Rice Husk Ash. *Biomass Bioenergy* **2011**, *35*, 1227−1234.
(6) Basta, A.; Fierro, V.; El-Saied, H.; Celzard, A. 2-Steps Koh Activation of Rice Straw: An Efficient Method for Preparing High-Performance Activated Carbons. *Bioresour. Technol.* **2009**, *100*, 3941−3947.
(7) Gao, P.; Liu, Z.-h.; Xue, G.; Han, B.; Zhou, M.-h. Preparation and Characterization of Activated Carbon Produced from Rice Straw by (Nh 4) 2 Hpo 4 Activation. *Bioresour. Technol.* **2011**, *102*, 3645−3648.
(8) Hu, S.; Hsieh, Y.-L. Preparation of Activated Carbon and Silica Particles from Rice Straw. *ACS Sustainable Chem. Eng.* **2014**, *2*, 726−734.

DOI: 10.1021/acssuschemeng.5b00600
ACS Sustainable Chem. Eng. 2016, 4, 728−737

(9) Hessien, M.; Rashad, M.; Zaky, R.; Abdel-Aal, E.; El-Barawy, K. Controlling the Synthesis Conditions for Silica Nanosphere from Semi-Burned Rice Straw. *Mater. Sci. Eng., B* **2009**, *162*, 14−21.
(10) Kadam, K. L.; Forrest, L. H.; Jacobson, W. A. Rice Straw as a Lignocellulosic Resource: Collection, Processing, Transportation, and Environmental Aspects. *Biomass Bioenergy* **2000**, *18*, 369−389.
(11) Karimi, K.; Emtiazi, G.; Taherzadeh, M. J. Production of Ethanol and Mycelial Biomass from Rice Straw Hemicellulose Hydrolyzate by Mucor Indicus. *Process Biochem.* **2006**, *41*, 653−658.
(12) Sangnark, A.; Noomhorm, A. Chemical, Physical and Baking Properties of Dietary Fiber Prepared from Rice Straw. *Food Res. Int.* **2004**, *37*, 66−74.
(13) Xiao, B.; Sun, X. F.; Sun, R. Chemical, Structural, and Thermal Characterizations of Alkali-Soluble Lignins and Hemicelluloses, and Cellulose from Maize Stems, Rye Straw, and Rice Straw. *Polym. Degrad. Stab.* **2001**, *74*, 307−319.
(14) Reddy, N.; Yang, Y. Q. Properties of High-Quality Long Natural Cellulose Fibers from Rice Straw. *J. Agric. Food Chem.* **2006**, *54*, 8077−8081.
(15) Adel, A. M.; El-Wahab, Z. H. A.; Ibrahim, A. A.; Al-Shemy, M. T. Characterization of Microcrystalline Cellulose Prepared from Lignocellulosic Materials. Part Ii: Physicochemical Properties. *Carbohydr. Polym.* **2011**, *83*, 676−687.
(16) Adel, A. M.; El-Wahab, Z. H. A.; Ibrahim, A. A.; Al-Shemy, M. T. Characterization of Microcrystalline Cellulose Prepared from Lignocellulosic Materials. Part I. Acid Catalyzed Hydrolysis. *Bioresour. Technol.* **2010**, *101*, 4446−4455.
(17) El-Sakhawy, M.; Hassan, M. L. Physical and Mechanical Properties of Microcrystalline Cellulose Prepared from Agricultural Residues. *Carbohydr. Polym.* **2007**, *67*, 1−10.
(18) Abe, K.; Yano, H. Comparison of the Characteristics of Cellulose Microfibril Aggregates of Wood, Rice Straw and Potato Tuber. *Cellulose* **2009**, *16*, 1017−1023.
(19) Lu, P.; Hsieh, Y. L. Preparation and Characterization of Cellulose Nanocrystals from Rice Straw. *Carbohydr. Polym.* **2012**, *87*, 564−573.
(20) Jiang, F.; Hsieh, Y.-L. Holocellulose Nanocrystals: Amphiphilicity, Oil/Water Emulsion, and Self-Assembly. *Biomacromolecules* **2015**, *16*, 1433−41.
(21) Jiang, F.; Han, S.; Hsieh, Y.-L. Controlled Defibrillation of Rice Straw Cellulose and Self-Assembly of Cellulose Nanofibrils into Highly Crystalline Fibrous Materials. *RSC Adv.* **2013**, *3*, 12366−12375.
(22) Jiang, F.; Hsieh, Y. L. Chemically and Mechanically Isolated Nanocellulose and Their Self-Assembled Structures. *Carbohydr. Polym.* **2013**, *95*, 32−40.
(23) Gu, J.; Hsieh, Y.-L. Surface and Structure Characteristics, Self-Assembling, and Solvent Compatibility of Holocellulose Nanofibrils. *ACS Appl. Mater. Interfaces* **2015**, *7*, 4192−4201.
(24) Nie, X.-N.; Liu, J.; She, D.; Sun, R.-C.; Xu, F. Physicochemical and Structural Characterization of Hemicelluloses Isolated by Different Alcohols from Rice Straw. *BioResources* **2013**, *8*, DOI: 10.15376/biores.8.3.3817-3832.
(25) Goksu, E. I.; Karamanlioglu, M.; Bakir, U.; Yilmaz, L.; Yilmazer, U. Production and Characterization of Films from Cotton Stalk Xylan. *J. Agric. Food Chem.* **2007**, *55*, 10685−10691.
(26) Bodin, A.; Ahrenstedt, L.; Fink, H.; Brumer, H.; Risberg, B.; Gatenholm, P. Modification of Nanocellulose with a Xyloglucan−Rgd Conjugate Enhances Adhesion and Proliferation of Endothelial Cells: Implications for Tissue Engineering. *Biomacromolecules* **2007**, *8*, 3697−3704.
(27) Jain, A.; Gupta, Y.; Jain, S. K. Perspectives of Biodegradable Natural Polysaccharides for Site-Specific Drug Delivery to the Colon. *J. Pharm. Pharm. Sci.* **2007**, *10*, 86−128.
(28) Vandamme, T. F.; Lenourry, A.; Charrueau, C.; Chaumeil, J. The Use of Polysaccharides to Target Drugs to the Colon. *Carbohydr. Polym.* **2002**, *48*, 219−231.
(29) Mikkonen, K. S.; Tenkanen, M. Sustainable Food-Packaging Materials Based on Future Biorefinery Products: Xylans and Mannans. *Trends Food Sci. Technol.* **2012**, *28*, 90−102.
(30) de Azeredo, H. M. Nanocomposites for Food Packaging Applications. *Food Res. Int.* **2009**, *42*, 1240−1253.
(31) Hon, D. N.-S.; Shiraishi, N. *Wood and Cellulosic Chemistry*, 2nd ed.; Marcel Dekker, Inc: New York, 2001.
(32) Gordobil, O.; Egüés, I.; Urruzola, I.; Labidi, J. Xylan−Cellulose Films: Improvement of Hydrophobicity, Thermal and Mechanical Properties. *Carbohydr. Polym.* **2014**, *112*, 56−62.
(33) Hansen, N. M. L.; Blomfeldt, T. O. J.; Hedenqvist, M. S.; Plackett, D. V. Properties of Plasticized Composite Films Prepared from Nanofibrillated Cellulose and Birch Wood Xylan. *Cellulose* **2012**, *19*, 2015−2031.
(34) Mikkonen, K. S.; Pitkanen, L.; Liljestrom, V.; Bergstrom, E. M.; Serimaa, R.; Salmen, L.; Tenkanen, M. Arabinoxylan Structure Affects the Reinforcement of Films by Microfibrillated Cellulose. *Cellulose* **2012**, *19*, 467−480.
(35) Peng, X. W.; Ren, J. L.; Zhong, L. X.; Sun, R. C. Nanocomposite Films Based on Xylan-Rich Hemicelluloses and Cellulose Nanofibers with Enhanced Mechanical Properties. *Biomacromolecules* **2011**, *12*, 3321−3329.
(36) Saxena, A.; Elder, T. J.; Pan, S.; Ragauskas, A. J. Novel Nanocellulosic Xylan Composite Film. *Composites, Part B* **2009**, *40*, 727−730.
(37) Saxena, A.; Elder, T. J.; Ragauskas, A. J. Moisture Barrier Properties of Xylan Composite Films. *Carbohydr. Polym.* **2011**, *84*, 1371−1377.
(38) Sun, Q. N.; Mandalika, A.; Elder, T.; Nair, S. S.; Meng, X. Z.; Huang, F.; Ragauskas, A. J. Nanocomposite Film Prepared by Depositing Xylan on Cellulose Nanowhiskers Matrix. *Green Chem.* **2014**, *16*, 3458−3462.
(39) Siqueira, G.; Bras, J.; Dufresne, A. Cellulose Whiskers Versus Microfibrils: Influence of the Nature of the Nanoparticle and Its Surface Functionalization on the Thermal and Mechanical Properties of Nanocomposites. *Biomacromolecules* **2009**, *10*, 425−32.
(40) Jiang, F.; Kondo, T.; Hsieh, Y.-L. Rice Straw Cellulose Nanofibrils via Aqueous Counter Collision and Differential Centrifugation and Their Self-Assembled Structures. *ACS Sustainable Chem. Eng.* **2016**, DOI: 10.1021/acssuschemeng.5b01653.
(41) Segal, L.; Creely, J. J.; Martin, A. E.; Conrad, C. M. An Empirical Method for Estimating the Degree of Crystallinity of Native Cellulose Using the X-Ray Diffractometer. *Text. Res. J.* **1959**, *29*, 786−794.
(42) Klug, H. P.; Alexander, L. E. *X-Ray Diffraction Procedures for Polycrystalline and Amorphous Materials*; Wiley Interscience: New York, 1954.
(43) Hu, S.; Hsieh, Y. L. Ultrafine Microporous and Mesoporous Activated Carbon Fibers from Alkali Lignin. *J. Mater. Chem. A* **2013**, *1*, 11279−11288.
(44) Cagnon, B.; Py, X.; Guillot, A.; Stoeckli, F.; Chambat, G. Contributions of Hemicellulose, Cellulose and Lignin to the Mass and the Porous Properties of Chars and Steam Activated Carbons from Various Lignocellulosic Precursors. *Bioresour. Technol.* **2009**, *100*, 292−298.
(45) Hu, S.; Hsieh, Y.-L. Ultrafine Microporous and Mesoporous Activated Carbon Fibers from Alkali Lignin. *J. Mater. Chem. A* **2013**, *1*, 11279−11288.
(46) El Mansouri, N.-E.; Salvadó, J. Structural Characterization of Technical Lignins for the Production of Adhesives: Application to Lignosulfonate, Kraft, Soda-Anthraquinone, Organosolv and Ethanol Process Lignins. *Ind. Crops Prod.* **2006**, *24*, 8−16.
(47) Hanaoka, T.; Inoue, S.; Uno, S.; Ogi, T.; Minowa, T. Effect of Woody Biomass Components on Air-Steam Gasification. *Biomass Bioenergy* **2005**, *28*, 69−76.
(48) Grondahl, M.; Eriksson, L.; Gatenholm, P. Material Properties of Plasticized Hardwood Xylans for Potential Application as Oxygen Barrier Films. *Biomacromolecules* **2004**, *5*, 1528−1535.
(49) Hoije, A.; Grondahl, M.; Tommeraas, K.; Gatenholm, P. Isolation and Characterization of Physicochemical and Material Properties of Arabinoxylans from Barley Husks. *Carbohydr. Polym.* **2005**, *61*, 266−275.

DOI: 10.1021/acssuschemeng.5b00600
ACS Sustainable Chem. Eng. 2016, 4, 728−737

(50) Mikkonen, K. S.; Heikkinen, S.; Soovre, A.; Peura, M.; Serimaa, R.; Talja, R. A.; Helén, H.; Hyvönen, L.; Tenkanen, M. Films from Oat Spelt Arabinoxylan Plasticized with Glycerol and Sorbitol. *J. Appl. Polym. Sci.* **2009**, *114*, 457−466.
(51) Kayserilioğlu, B. Ş.; Bakir, U.; Yilmaz, L.; Akkaş, N. Use of Xylan, an Agricultural by-Product, in Wheat Gluten Based Biodegradable Films: Mechanical, Solubility and Water Vapor Transfer Rate Properties. *Bioresour. Technol.* **2003**, *87*, 239−246.
(52) Jiang, F.; Hsieh, Y.-L. Assembling and Redispersibility of Rice Straw Nanocellulose: Effect of Tert-Butanol. *ACS Appl. Mater. Interfaces* **2014**, *6*, 20075−20084.

DOI: 10.1021/acssuschemeng.5b00600
ACS Sustainable Chem. Eng. 2016, 4, 728−737